Bioorg. Med. Chem. 28 (2020) 115817

Contents lists available at ScienceDirect

Bioorganic & Medicinal Chemistry

journal homepage: www.elsevier.com/locate/bmc

One-step partial synthesis of (±)-asperteretone B and related *h*PTP1B$_{1–400}$ inhibitors from butyrolactone I

José Rivera-Chávez [a,*], Diego Coporo-Blancas [a], Jesús Morales-Jiménez [b]

[a] Departamento de Productos Naturales, Instituto de Química, Universidad Nacional Autónoma de México, Ciudad Universitaria 04510, Ciudad de México, Mexico
[b] CONACYT-Consorcio de Investigación, Innovación y Desarrollo para las Zonas Áridas (CIIDZA), Instituto Potosino de Investigación Científica y Tecnológica A. C., Camino a la Presa San José 2055, Lomas 4a sección, 78216 San Luis Potosí, Mexico

ARTICLE INFO

Keywords:
Full-length PTP1B
Semisynthesis
Krapcho decarboxylation
Fungal natural products
Butyrolactone I

ABSTRACT

Protein tyrosine phosphatase 1B (PTP1B) is a validated target for developing antiobesity, antidiabetic and anticancer drugs. Over the past years, several inhibitors of PTP1B have been discovered; however, none has been approved by the drug regulatory agencies. Interestingly, the research programs focused on discovering PTP1B inhibitors typically use truncated structures of the protein (PTP1B$_{1-300}$, 1–300 amino acids), leading to the loss of valuable information about the inhibition and selectivity of ligands and repeatedly misleading the optimization of putative drug leads. Up to date, only six inhibitors of the full-length protein (*h*PTP1B$_{1-400}$), with affinity constants ranging from 1.3×10^4 to 3.3×10^6 M^{-1}, have been reported. Towards the discovery of new ligands of the full-length human PTP1B (*h*PTP1B$_{1-400}$) from natural sources, herein we describe the isolation of a γ-lactone (**1**, butyrolactone I) from the fungus *Aspergillus terreus*, as well as the semisynthesis, inhibitory properties (*in vitro* and *in silico*), and the structure-activity relationship of a set of butyrolactone derivatives (**1** and **2**, and **6–12**) as *h*PTP1B$_{1-400}$ inhibitors, as well as the affinity constant ($k_a = 2.2 \times 10^5$ M^{-1}) of the **1**-*h*PTP1B$_{1–400}$ complex, which was determined by fluorescence quenching experiments, after the inner filter effect correction.

1. Introduction

Protein tyrosine phosphatase 1B (PTP1B) has recently emerged as a target for developing antiobesity, antidiabetic and anticancer drugs. In diabetes and obesity, it negatively regulates the insulin and leptin signal transduction pathways, respectively, enhancing the insulin receptor's susceptibility and stimulating glucose transporters translocation and glucose uptake in insulin-sensitive cells.[1] Whereas in cancer it controls several pathways involved in tumor growth, tumorigenesis, and metastasis, for example, the Ras/Raf/MAPK and PI3K/AKT pathways.[2,3]

Since the validation of PTP1B as a target to treat chronic diseases, numerous programs have focused on the synthesis or isolation (from natural sources) of both competitive and non-competitive inhibitors.[4] Such programs have resulted in the discovery of more than 500 PTP1B$_{1-300}$ inhibitors.[5] Two of the most promising drugs developed to date are ertiprotafib (a competitive inhibitor of the truncated model, PTP1B$_{1-300}$), and trodusquemine, a non-competitive inhibitor of the full-length protein (1–405 residues). However, while both advanced to phase II clinical trials, they were discontinued due to their low selectivity, adverse effects, and/or pharmacokinetic properties.[6] In a recent study, it was demonstrated that the use of truncated structures of this protein (*h*PTP1B$_{1-300}$) in drug discovery programs lead to the loss of valuable information about the inhibition and selectivity of the ligands, which could be associated with the low rate of success of PTP1B inhibitors.[7]

The discovery of an allosteric site in PTP1B, and the expression of a full-length protein (1–400 amino acids) have shifted the approaches to discover inhibitors. The allosteric site in PTP1B is a hydrophobic pocket constituted by helices α3, α6, and α7, situated on the C-terminus of the protein and located 20 Å away from the catalytic domain.[8] This pocket regulates the catalytic domain's flexibility, which results in a decrease of the phosphatase activity.[8–10] Whereas the C-terminal domain of this protein has lower sequence conservation and higher specificity,[9] significantly increasing the chances of discovering more specific molecules with less toxic effects.

Thus, as part of our ongoing research program focused on discovering non-competitive inhibitors of *h*PTP1B$_{1–400}$ from natural sources, particularly from fungi, the bioactive extract of an *Aspergillus terreus* (IQ-046) was chemically investigated. This study led to the isolation of butyrolactone I (**1**), butyrolactone IV (**2**), lovastatin (**3**), methyl 3,4,5-trimethoxy-2-(2-(nicotinamido)benzamido)benzoate (**4**), and

* Corresponding author.
E-mail address: jrivera@iquimica.unam.mx (J. Rivera-Chávez).

https://doi.org/10.1016/j.bmc.2020.115817
Received 2 September 2020; Received in revised form 1 October 2020; Accepted 8 October 2020
Available online 15 October 2020

chrysamide B (**5**), exhibiting the privileged metabolic potential of this strain. Furthermore, the biological properties of compounds **1** and **2** as *h*PTP1B$_{1–400}$ inhibitors were screened *in vitro*, displaying IC_{50} values of 35 and higher than 450 μM, respectively. Motivated by the differences in biological activity of compounds **1** and **2**, several semisynthetic derivatives of **1** [asperteretone B (**6**), (±)-5″-iodoasperteretone B (**7**), (±)-asperteretone D (**8**), aspernolide A (**9**), 4′,4″-butyrolactone I dipropionate (**10**), $\Delta^{7'',8''}$-9″-hydroxy-4′,4″-butyrolactone I dipropionate (**11**), and 3′,5′,5″,8″-tetrabromoaspernolide A (**12**)] were prepared via one-step reactions. Principal component analysis of the chemical space of butyrolactone I (**1**) derivatives allowed a structure-activity relationship to be established, indicating that small differences in these ligands' structure significantly affect their IC_{50} values. Molecular docking studies of butyrolactone I (**1**) and its derivatives with a homologated model of *h*PTP1B$_{1–400}$ indicated that compounds (**1**, **2**, and **6–12**) bind to four different sites within the protein. Three of them in the macromolecule's C-terminal domain, suggesting that some of them may behave as allosteric modulators. Finally, after inner filter effect correction, fluorescence quenching experiments determined the binding affinity of the complex **1**-*h*PTP1B$_{1–400}$ and supported that butyrolactone I (**1**) may behave as an allosteric inhibitor of the protein.

2. Results and discussion

2.1. Isolation of natural products from Aspergillus terreus IQ-046

The extract of *Aspergillus terreus* (IQ-046, Fig. S1, Supporting Information) was pursued for chemical investigation, as it inhibited the activity of *h*PTP1B$_{1–400}$ in an *in vitro* assay (95% inhibition at 50 ppm). Fractionation of the extract led to the isolation of butyrolactone I and IV (**1** and **2**),[11,12] lovastatin (**3**, mevinolin),[13] methyl 3,4,5-trimethoxy-2-(2-(nicotinamido)benzamido)benzoate (**4**),[14] and chrysamide B (**5**). The latter being a nitro-compound previously isolated from *Penicillium chrysogenum* SCSIO41001 (Fig. 1).[15,16] All compounds were characterized by comparing their spectroscopic and spectrometric data with those previously described in the literature (Figs. S2–S28, Supporting Information). *In vitro* biological evaluation of compounds **1** and **2** as *h*PTP1B$_{1-400}$ inhibitors (IC_{50} = 35 and >450 μM, respectively) triggered our interest in the structure-activity relationship (SAR) of these molecules.

2.2. Partial synthesis of butyrolactone I (1) derivatives (6–12)

Thus, to explore the reactivity of butyrolactone I (**1**, the most abundant compound in the extract of IQ-046), and to expand the chemical space of this interesting bioactive metabolite, several one-step reactions were performed (Scheme 1). Considering the features of compound **1**, it was initially speculated that the 4′, 4″ phenolic groups could be methylated using diazomethane or iodomethane. Unfortunately, these methodologies did not result in the methylation of the product. Instead, diazomethane generated an unstable methylated product at the 4-OH position, while iodomethane was unreactive. Challenged by these results, we hypothesized that **1** could be methylated at the 4′, 4″ phenolic groups using dimethyl carbonate (DMC), and tetrabutylammonium iodide (TBAI).[17] Interestingly, under our reaction settings, the dimethylated product was not obtained. Instead, two decarboxylated products of **1** were generated, as evidenced by the ^{1}H NMR, ^{13}C NMR, and HR-DART-MS data (Figs. S29–S31, and S34–S36, for compounds **6** and **7**, respectively, Supporting Information). Careful analysis of the 1D and 2D NMR (Figs. S32–S33, and S37–S38, respectively, Supporting Information) and the CD data (Fig. S64, Supporting Information) established the structure of the decarboxylated products as (±)-asperteretone B (**6**), a secondary metabolite recently isolated from *Aspergillus terreus*,[18] and its 5″-iodo derivative (**7**). Further insights about the formation of compound **6** from **1** were obtained by dissolving the later in THF, THF-DMC, and THF-TBAI, and heated up to 80 °C from six to 60 h. Interestingly, compounds **6** or **7** were not obtained under these conditions, indicating they are generated via a one-pot reaction involving TBAI and DMC. Mechanistically, compound **6** could be produced from **1** via opening and methylation of the γ-lactone ring, mediated by methoxide -generated *in situ* through a bimolecular base-catalyzed alkyl cleavage mechanism ($B_{AI}2$)-,[19] and a re-arrangement of the γ-lactone, followed by a Krapcho-like[20] decarboxylation process (Scheme 2).

(±)-5″-Iodoasperteretone B (**7**) was isolated as a white amorphous powder. Its molecular formula was established as $C_{23}H_{23}O_5I$, based on HR-DART-MS data ($[M+H]^+$ m/z = 507.0681, calcd. for $C_{23}H_{24}O_5I$, Δ = +3.5 ppm), (Fig. S34, Supporting Information), indicating an index of hydrogen deficiency of 12. The ^{1}H and ^{13}C NMR spectra (Figs. S35 and S36, Supporting Information) were similar to those obtained for **6**. The main differences were observed in the aromatic region, particularly the loss of the doublet attributed to the 5″-H at δ_H = 6.75 ppm, the change in

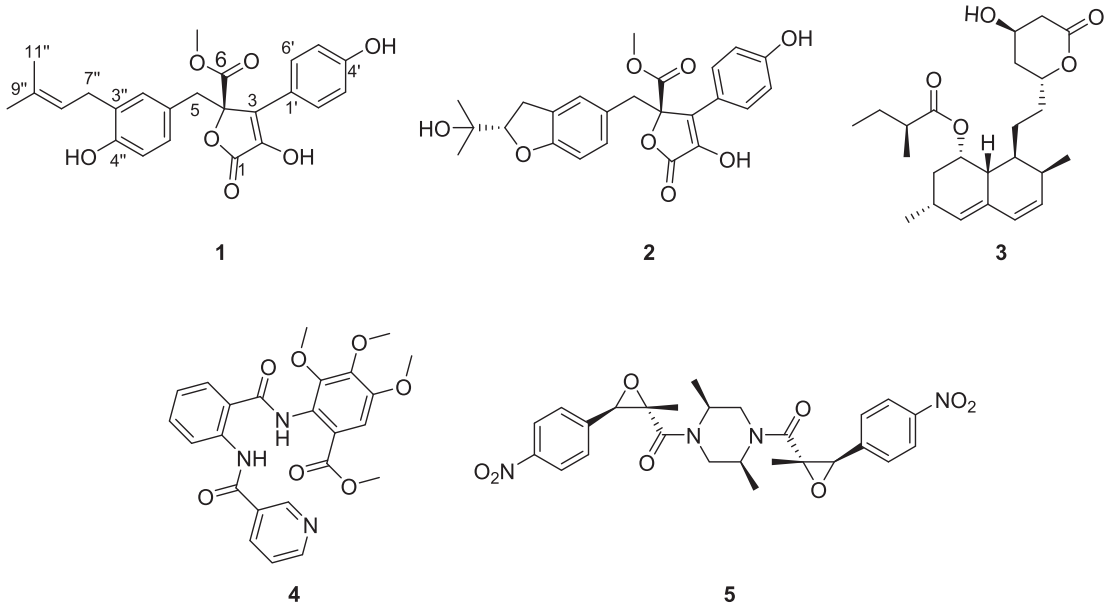

Fig. 1. Structure of compounds isolated from *A. terreus* (IQ-046).

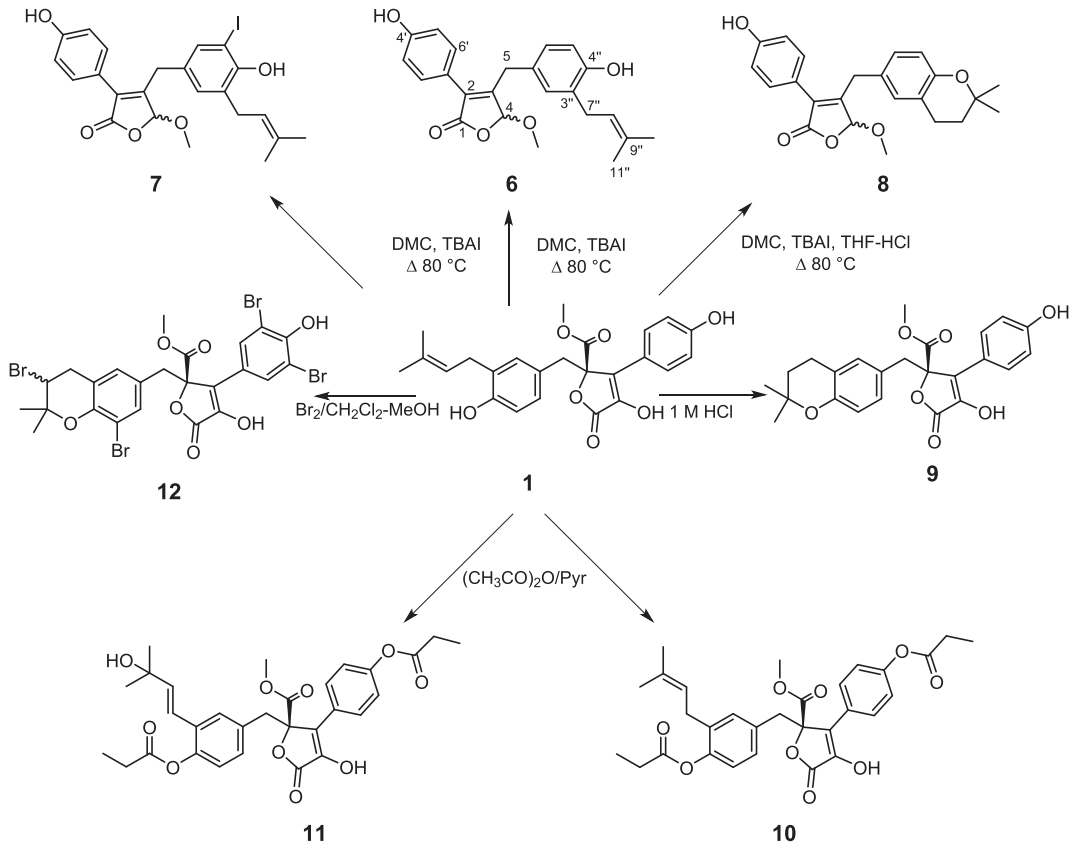

Scheme 1. Semisynthesis of compounds **6–12**.

the coupling pattern from an ABB' system in **6** to an AB system in **7** (Table S1, Supporting Information), and the shielding of the C-5″ from δ_C 116.3 in **6** to 86.4 in **7** (Table S2, Supporting Information).

Compound **8** was obtained by reacting **1** with DMC and TBAI in acidified (HCl) THF at 80 °C. The ^{1}H, ^{13}C NMR, and HR-ESI-MS data (Figs. S39–S41, Supporting Information) agreed with those previously reported.[18] Further analysis of the 2D NMR spectra (Figs. S42 and S43, Supporting Information) confirmed the structure of **8** as (±)-asperteretone D.

Asperteretones B and D (**6** and **8**) were recently isolated as racemic mixtures from the extract of a coral-associated *A. terreus*. Both the 4*S* and 4*R* enantiomers of **6** and **8** showed potent α-glucosidase inhibitory activity (a molecular target for treating type II diabetes mellitus), with IC_{50} values ranging from 15.7 to 19.2 μM.[18] Remarkably, Liu and coworkers proposed the structures of **6** and **8** as corrections of the previously described (±)-asperteretal D, and (4*S*)-4-decarboxylflavipesolide C,[21] two specialized metabolites obtained from a different strain of *A. terreus* (OUCMDZ-2739), grown under static conditions in liquid media supplemented with 10 μM trichostatin A.

Compound **9** was obtained by reacting **1** with 1 M HCl at rt. The ^{1}H, ^{13}C NMR, and HR-ESI-MS data (Figs. S44–S46, Supporting Information) were in agreement with those previously reported.[22] Additional analysis of the 2D NMR spectra (Figs. S47 and S48, Supporting Information) confirmed the structure of **9** as aspernolide A.

To explore the reactivity of the phenolic groups at 4′ and 4″ in compound **1**, it was reacted with propionic anhydride in pyridine (Scheme 1). As expected,[23] the 4′,4″-butyrolactone I dipropionate (**10**) was obtained, as evidenced by the ^{1}H, ^{13}C, HSQC, and HMBC NMR spectra, and the HR-ESI-MS data (Figs. S49–S53, Supporting Information). Interestingly, under the reaction conditions, a second product was generated (**11**). The 1D, 2D NMR, and the HR-ESI-MS data (Figs. S54–S56, Supporting Information) of this compound resembled those of product **10**. The main differences were the presence of an *E*-double bound and an oxygenated sp^3 carbon (C-9″). Thoughtful inspection of the HMBC spectrum (Fig. S58, Supporting Information) established the structure of **11** as $\Delta^{7'',8''}$-9″-hydroxy-4′,4″-butyrolactone I dipropionate.

Unsurprisingly, nature has demonstrated that the incorporation of halogens (Cl, Br, and I) onto the scaffolds of organic compounds is a typical process. Up to date, more than 5000 halogenated natural products with numerous exciting activities have been reported in the literature. [24] In this regard, chlorination and bromination are routine modifications in natural products' structural diversification, since halogens play a crucial role in bioactivity by increasing the affinity and selectivity of molecules for their targets.[25–30] This phenomenon is mainly associated with the ability of these atoms to interact with biomacromolecules by halogen bonding (interactions of the type R–X···Y–R', where X acts as a Lewis acid and Y is an electron donor atom),[29] as well as their capacity to increase the lipophilicity and steric hindrance.[30] In fact, the success of pairing halogens with bioactive organic molecules has led to a growing trend in the number of iodinated and brominated drugs reaching clinical phases.[31] Conversely, some aryl bromides have been associated with the occurrence of hepatotoxicity,[32] whereas the presence of iodide in medicines or foods is related with hypersensitivity and thyroids diseases,[33] this stigma (high toxicity) have seriously limited the research in this field, limiting our understanding of the biological properties of halogen-containing natural products. Considering the positive impact of halogenation on the bioactivity of organic compounds, the 3′,5′,5″,8″-tetrabrominated analog of aspernolide A (**12**) was prepared reacting **1** with Br_2 in a 1:1 MeOH-CH_2Cl_2 mixture at rt. Compound **12** was obtained as a white amorphous powder. Its molecular formula was established as $C_{24}H_{20}O_7Br_4$ based on the isotopic pattern and the HR-ESI-MS data ($[M-H]^-$ = 734.7877 *m/z*, calculated for $C_{24}H_{19}O_7Br_4$, Δ = 1.0 ppm) (Fig. S59, Supporting Information), indicating an index of hydrogen deficiency of 13. The ^{1}H spectrum (Fig. S60, Supporting Information) displayed signals

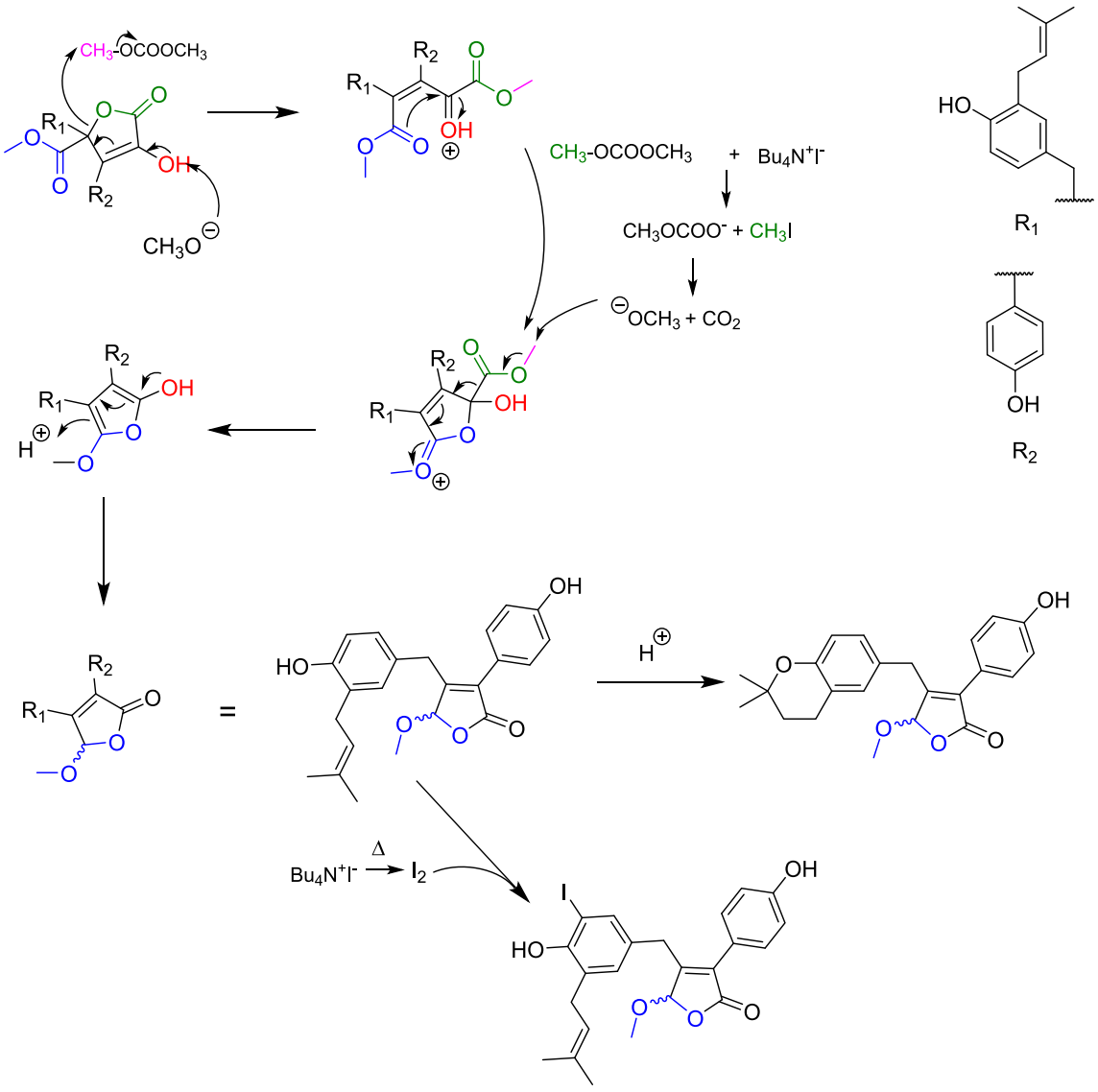

Scheme 2. Proposed mechanism of reaction for the formation of (±)-asperteretone B (**6**), (±)-5″-iodoasperteretone B (**7**), and (±)-asperteretone D (**8**).

attributable to an A_2 spin system (δ_H 7.79), an aromatic AB system (δ_H 6.83 and 6.55), an oxymethylene (δ_H 3.51 and 3.34), an AMX spin system (δ_H 4.18, 3.26 and 3.10), a methoxy (δ_H 3.83) and two methyl groups (δ_H 1.55 and 1.40). The ^{13}C NMR, together with the HSQC and HMBC (Figs. S61–S63, Supporting Information) experiments, further confirmed the structure of compound **12**.

2.3. *h*PTP1B$_{1–400}$ inhibition and principal components analysis (PCA)

PTP1B has gained significant interest since its validation as a target for developing anti-obesity, antidiabetic, and anticancer drugs.[1] Recently, we reported the expression and purification of a full-length human PTP1B (*h*PTP1B$_{1–400}$), as we detected a gap in the literature regarding the use of truncated models of this macromolecule in drug discovery programs (both *in vitro* or *in silico*). The use of these models often leads to the loss of valuable information about the mechanisms of inhibition and selectivity of ligands, while simultaneously misleading the optimization of putative drug leads. In a recent report, four dimeric phenalenones isolated from an ant-hill associated *Talaromyces* sp. were reported as putative allosteric modulators of *h*PTP1B$_{1–400}$, being only the second class of inhibitors of the full-length enzyme reported in the literature.[34]

To gain further insights about the potential of compounds **1**, **2**, and **6–12** as *h*PTP1B$_{1–400}$ inhibitors, these molecules were evaluated *in vitro* to determine the effect of the introduced or eliminated fragments on the hydrolase activity of the protein (Fig. 2 and Table 1). Compounds **2**, **8**, and **9** showed moderate to weak activity with IC_{50} values ranging from

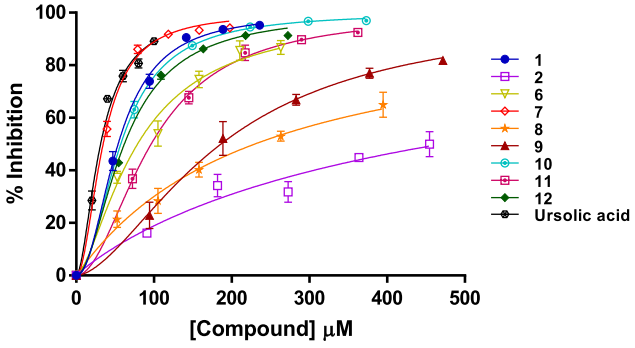

Fig. 2. Concentration-response curves for enzymatic inhibitory activity of compounds **1**, **2**, **6–12**, and ursolic acid (positive control) against *h*PTP1B$_{1-400}$. These data correspond to three independent experiments.

Table 1
Experimental IC_{50} values for compounds **1**, **2**, and **6–12** as *h*PTP1B$_{1–400}$ inhibitors.

compound	IC_{50} (μM)
1	53.9 ± 1.1
2	>450
6	78.8 ± 3.6
7	34.6 ± 1.0
8	229.4 ± 9.8
9	186.1 ± 4.9
10	57.3 ± 1.3
11	96.3 ± 1.9
12	61.8 ± 1.4
Ursolic acid	33.1 ± 1.8

186 to higher than 450 μM, while products **6**, **7**, and **10–12** displayed IC_{50} values from 35 to 97 μM, similar to that of ursolic acid, an allosteric inhibitor of the full-length protein (IC_{50} = 33.1 μM, positive control), duclauxin, xenoclauxin, bacillisporin G, and talaromycesone B, which display IC_{50} values ranging from 12.7 to 82.1 μM.[7]

Up to date, several natural and semisynthetic triterpenes (ursolic, moronic, and oleanolic acids)[35–37] have been reported as inhibitors of the truncated model of PTP1B. These molecules inhibit the protein's phosphatase activity by binding to an extended allosteric site, or directly interacting with the catalytic domain, as predicted by docking studies and demonstrated by kinetics experiments.[35–37] Additionally, numerous PTP1B$_{1-300}$ inhibitors with different scaffolds, including γ and δ-lactones, have been isolated from fungi. Some examples include chrysopyrones (competitive inhibitors),[38] deflectins,[39] tylopilusin D (non-competitive inhibitor),[40] betulactone B,[41] and verruculide B,[42] highlighting the versatility of fungi to produce small molecules with PTP1B inhibitory properties. Moreover, it does high point the affinity of these structural moieties (γ and δ-lactones) for the macromolecule.

To explore the chemical space of natural (**2**) and semisynthetic derivatives (**6–12**) of **1**, detect the critical topologies that impact the inhibition of the phosphatase activity of *h*PTP1B$_{1–400}$, and to establish a SAR, principal component analysis (PCA) of 14 analogs (Fig. S65, Supporting Information) was carried out. With this purpose, the number of rotatable bonds, the polar component of the solvent-accessible surface area (WPSA), the estimated number of hydrogen bonds that would be accepted (accptHB), the polar surface area (PSA), the number of N and O atoms (#NandO), the number of atoms in rings, and the number of ring atoms not able to form conjugated aromatic systems, were predicted using QikProp. Additionally, the number of halogens, as well as the experimental IC_{50} values were considered. Principal components one and two (PC1 and PC2) explained 73.6% of the covariance, while PC1–PC3 described 96.1%. Remarkably, the number of rotatable bonds, the accptHB, the PSA, and #NandO, had the most significant contribution to PC1. In contrast, all the descriptors except for the number of rotatable bonds contributed to PC2. WPSA and the number of halogens significantly contributed to PC3.

The 2D representation of the PCA (PC1 vs. PC2, and PC1 vs. PC3, Fig. 3) revealed that active and poorly active analogs of **1** occupy different chemical space regions. For example, compounds that bear an isoprenyl group at C-3″ (**1**, **6a**, **6b**, **7a**, **7b**, **10**, and **11**, the most active products) grouped together, while separately clustered are the moderately active compounds **2a**, **2b**, **8a**, **8b**, and **9**, which lack this moiety.

2.4. Molecular docking

To gaining further structural insights about the putative binding mode of the butyrolactone I (**1**) analogs included in the PCA with *h*PTP1B$_{1–400}$, and explain the outcomes from bioactivity evaluation, docking studies were performed using a homologated model of the enzyme, as so far, there is no crystallographic structure reported for the full-length protein (Fig. 4). Initially, the performance of AutoDock (AD) was validated using trodusquemine, an aminosterol that binds to the C-terminal domain of *h*PTP1B$_{1–400}$ (Arg371, Arg373 and Val375 in α9′ and residues Leu299, His310, Ile311, Val334, and Ser393) with stoichiometry 2:1, and k_a values of 3.3×10^6 and 3.3×10^5 M^{-1}, respectively. The results from molecular coupling showed that AD successfully predicts the binding pocket of trodusquemine, which docked at the interface of both the N (Pro_{89}, Cys_{92}, Leu_{119}, Glu_{123}, Met_{133}, Ile_{134}, Phe_{135}, Glu_{136}, and Asp_{137}) and C-terminal (Thr_{368}, Glu_{369}, Val_{370}, Arg_{371}, and Ser_{372}) domains of the protein.

The docking of *h*PTP1B$_{1–400}$ with butyrolactone derivatives exhibited well-established bonds with amino acids in four different binding sites within the protein (Figs. 4, S67–S80, Supporting Information); three of them including residues of the C-terminal domain (residues 301–400). Interestingly, none of the molecules bonded to the active site of the enzyme. In all cases, the forces that governed the interactions were primarily hydrophobic (Van der Waals) and hydrogen bonding.

The putative binding site for compounds **1**, **2a**, **6a**, **6b**, **8a**, **8b**, **9**, and **12a** was formed by residues of the α1′ helix (Glu_4, Phe_7, Glu_8, Asp_{11}), the WPD loop (Ser_{187}, Pro_{188}, non-catalytic), the α3 helix (Ala_{189}), α6 and α7 helices (Leu_{272}, Ile_{275}, Glu_{276}, Lys_{279}, Val_{287}, Gln_{290}, Trp_{291}, Leu_{294}), and residues of the C-terminal domain (Cys_{324}, Glu_{326}, Phe_{327}, Phe_{328}, and

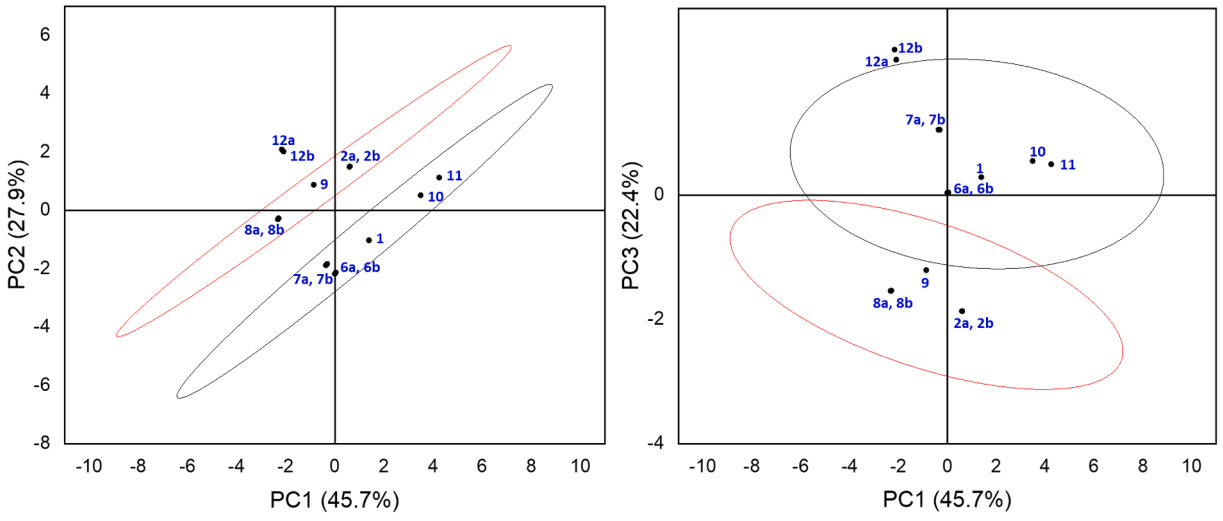

Fig. 3. Representation of the chemical space of natural butyrolactones (**1** and **2**), and semisynthetic analogs (**6–12**). The 2D plots were generated with the principal component analysis of nine descriptors. Components 1–3 described 96.1% of the covariance.

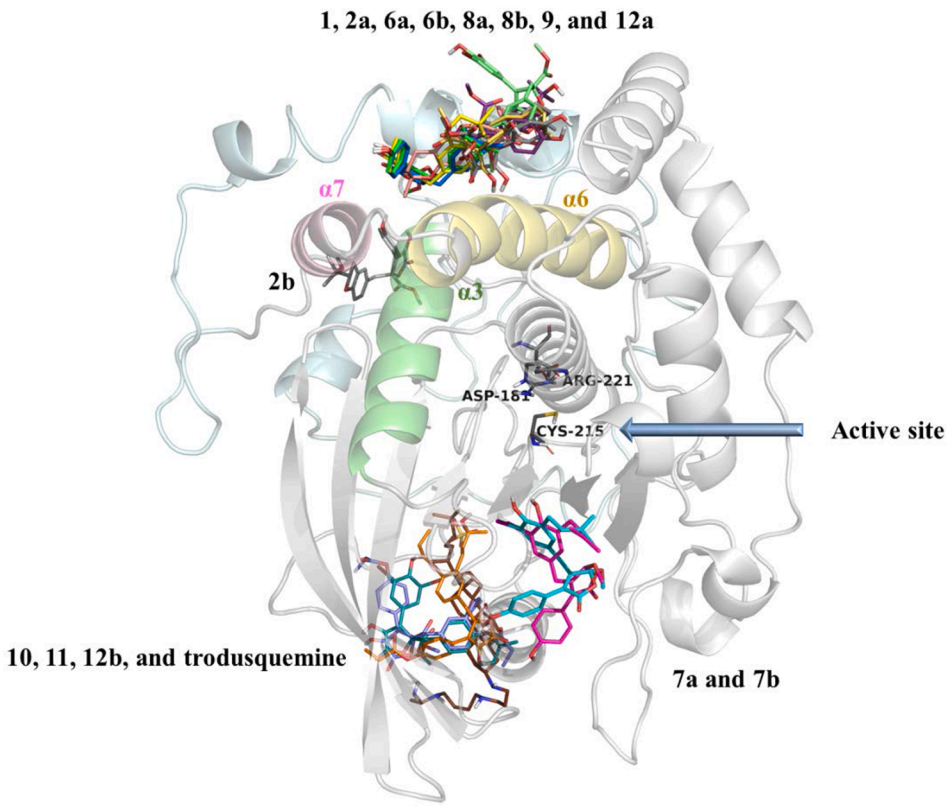

Fig. 4. 3D representation of the interaction of the complex **1**, **2a**, **2b**, **6a–12b**, and *h*PTP1B$_{1\text{-}400}$. In pale-cyan, the C-terminal domain of the protein (residues 300–400). In pale-green, the α3 helix (residues 189–201). In pale-yellow, the α6 helix (residues 265–281). In pale-pink, the α7 helix (residues 286–295). In black sticks, the residues involved in the catalytic triad (Asp$_{181}$, Cys$_{215}$, and Arg$_{221}$). In brown sticks trodusquemine. For clarity, the full-size images of the 3D models of the interaction of compounds **1**, **2a**, **2b**, and **6a–12b** in complex with *h*PTP1B$_{1\text{-}400}$ are provided in the Supporting Information file (Figs. S67–S80, Supporting Information). Graphics generated with PyMOL.

Val$_{334}$). The interaction of these molecules with residues of the allosteric site (helices α3, α6, and α7) and the C-terminus of *h*PTP1B$_{1–400}$, suggest that this set of ligands may induce conformational changes onto the protein and putatively behave as allosteric inhibitors. Conversely, the binding pocket for **2b** (4*R*, 8*S*, poorly active compound) was constructed by Lys$_{342}$, Cys$_{344}$, Pro$_{345}$, Asn$_{355}$, Ala$_{357}$, Pro$_{358}$, and Tyr$_{359}$, all of them residues of the C-terminal domain. These results indicated that the interaction of molecules with these amino acids, do not significantly affect the hydrolase activity of *h*PTP1B$_{1–400}$.

The union site for molecules **10**, **11**, and **12b** was similar to that predicted for trodusquemine. It consisted of residues of the α2 helix (Pro$_{89}$, Asn$_{90}$, Cys$_{92}$, Gly$_{93}$), *β* sheets 2–7 (Leu$_{119}$, Ala$_{122}$, Gln$_{123}$, Gln$_{127}$, Glu$_{132}$, Met$_{133}$, Ile$_{134}$, Phe$_{135}$, Asp$_{137}$), and one residue of the C-terminus of the protein (Thr$_{368}$), predicting a non-competitive type of inhibition. Interestingly, the acylation of the phenolic groups at C-4′ and C-4″ in **1** does not affect the bioactivity; however, these modifications direct compounds **10** and **11** to a different binding pocket within the protein, likely due to the conformational changes and steric hindrance imposed by the propionate moieties, which also form hydrogen bonds with Gln$_{123}$ stabilizing the interaction. In contrast, the binding site for compounds **7a** and **7b**, the most active compound of the series (iodinated), contained amino acids Leu$_{71}$, Lys$_{73}$, Gln$_{78}$, Arg$_{79}$, Ser$_{80}$, Glu$_{101}$, Gln$_{102}$, Lys$_{103}$, Ser$_{203}$, Leu$_{204}$, Ser$_{205}$, Pro$_{206}$, His$_{208}$, Glu$_{207}$, Gly$_{209}$, Pro$_{210}$, and Val$_{211}$, all of them residues from the *N*-terminal domain, and far away from the active site of the enzyme. Remarkably, these residues have 87% homology with TCPTP, which may compromise the *in vivo* selectivity of these molecules. Complementary studies are needed to support this statement fully.

Briefly, close inspection of the structures, bioactivity, PCA, and molecular docking data for the 14 analogs included in this study, revealed that (i) the isoprenyl group at C-3″ is a key feature for bioactivity, (ii) incorporation of bulky moieties onto the structure of **1** direct molecules to different binding sites within the protein, (iii) halogenation of **1** and its derivatives positively contributes to the bioactivity, (iv) incorporation of a hydroxy group at C-9″ (compounds **2** and **11**), and decarboxylation and re-arrangement of the γ-lactone negatively affect the phosphatase activity of *h*PTP1B$_{1\text{-}400}$ (Fig. 5). However, docking studies predicted two major binding pockets for this set of molecules within PTP1B$_{1\text{-}400}$, suggesting that the established structure-activity-relationship must be taken cautiously. Further experiments such as ^{1}H-^{15}N NMR TROSY and comparison of the IC$_{50}$ values of butyrolactone derivatives as inhibitors of the truncated and full-length protein are required to confirm the binding pockets and selectivity for these molecules experimentally.

2.5. *Steady-state fluorescence quenching experiments of hPTP1B$_{1\text{-}400}$ with butyrolactone I (1)*

To confirm the interaction of butyrolactone I (**1**, the most abundant product in the extract of *A. terreus* IQ-046) with *h*PTP1B$_{1–400}$, and support the outcomes from docking studies, steady-state fluorescence quenching experiments were carried out. The high sensitivity of tryptophan (Trp, a fluorescent amino acid) to its local environment results in changes in its emission spectra. This phenomenon allows for monitoring conformational transitions, subunit associations, and binding of a substrate or ligand, providing valuable insight into a protein's structure and function.[43,44] In this experiment, the Trp residues were used as intrinsic fluorophores. The samples were excited at 280 nm, and the emission spectra recorded from 300 to 500 nm. The marked reduction in the fluorescence intensity of *h*PTP1B$_{1–400}$ at increasing concentrations of compound **1** suggested that this molecule interacts with *h*PTP1B$_{1–400}$, inducing conformational changes that directly affect its phosphatase activity (allosteric inhibition, Fig. 6).

Furthermore, the affinity of the complex butyrolactone I (**1**)-*h*PTP1B$_{1–400}$ was measured (Fig. 6). Unsurprisingly, the well-known inner filter effect was observed by butyrolactone I (**1**), since it absorbs light at the excitation and emission wavelengths (Fig. S66, Supporting Information), which reduces the fluorescence emission of the

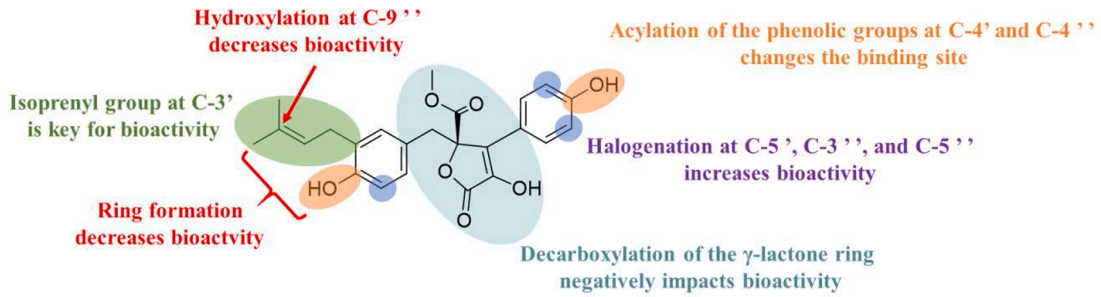

Fig. 5. Sites in **1** for bioactivity modulation.

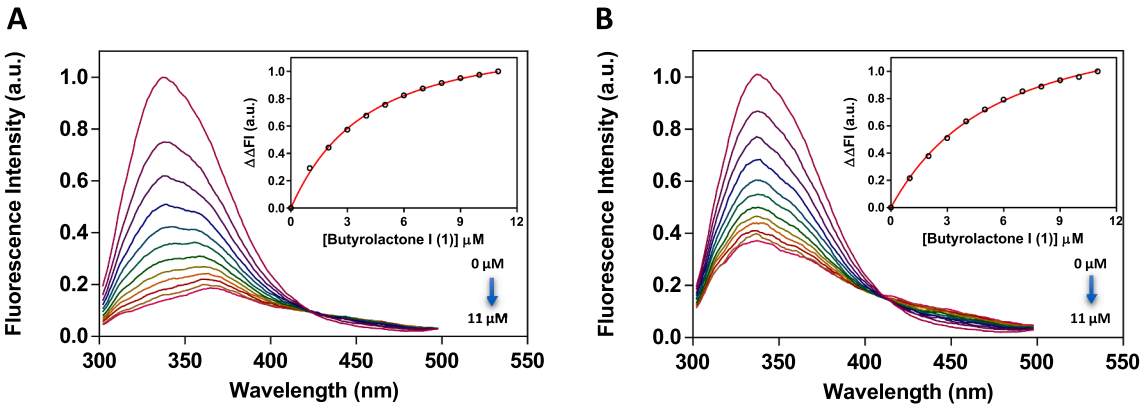

Fig. 6. (A) Fluorescence spectra and titration curve (insets) of *h*PTP1B$_{1–400}$ (0.5 μM) with increasing concentrations of butyrolactone I (**1**) (0–11 μM) before inner filter effect correction. (B) Fluorescence spectra and titration curve (inset) of *h*PTP1B$_{1–400}$ (0.5 μM) with increasing concentrations of butyrolactone I (**1**) (0–11 μM) upon inner filter effect correction. Samples were excited at 280 nm, and the emission spectra recorded from 300 to 500 nm. The changes in maximal fluorescence emission were corrected for light scattering and plotted against the total concentration of protein. The insets' red line comes from fitting the data to the binding model (Eq. (3)) to obtain the k_a ($1/k_d$). Experiments were carried out in HEPES 50 mM, NaCl 100 mM, and DTT 1.5 mM at pH 6.8.

complex.[43,45,46] The emission spectra of the *h*PTP1B$_{1–400}$, and **1**-*h*PTP1B$_{1–400}$ complex, before (Fig. 6A) and upon the inner filter effect correction (Fig. 6B) display a fluorescence quenching of 86.2% and 63.2%, respectively.[43–45] These data evidenced the strong absorption of butyrolactone I (**1**) at the excitation and emission wavelengths. Even though the concentration of **1** was low (11 μM), it created a significant inner filter effect and contributed 23% of the quenching.

The association constant (k_a) for the butyrolactone I (**1**)-*h*PTP1B$_{1–400}$ complex was calculated before (2.6×10^5 M^{-1}) and after (2.2×10^5 M^{-1}) the inner filter effect correction.[43–45] As expected, there are differences in the values, stressing the importance of the correction.[43,45,46] Butyrolactone I (**1**) showed higher affinity than ursolic acid (k_a of 1.3×10^4 M^{-1}),[47] and is comparable with the k_a reported for trodusquemine (3.3×10^5 M^{-1}).[34]

3. Conclusion

In summary, chemical investigation of the bioactive extract of *Aspergillus terreus* (IQ-046) as a *h*PTP1B$_{1–400}$ inhibitor led to the isolation of butyrolactone I (**1**), butyrolactone IV (**2**), lovastatin (**3**), methyl 3,4,5-trimethoxy-2-(2-(nicotinamido)benzamido)benzoate (**4**), and chrysamide B (**5**). Additionally, the reactivity of **1** was explored using one-step reactions, which allowed the semisynthesis of seven derivatives, including the recently reported (±)-asperteretone B (**6**) and (±)-asperteretone D (**8**), the known compound aspernolide A (**9**), as well as the four new derivatives (±)-5″-iodoasperteretone B (**7**), 4′,4″-butyrolactone I dipropionate (**10**), $\Delta^{7'',8''}$-9″-hydroxy-4′,4″-butyrolactone I dipropionate (**11**), and 3′,5′,5″,8″-tetrabromoaspernolide A (**12**). The biological properties of compounds **1**, **2**, and **6–12** as *h*PTP1B$_{1–400}$ inhibitors were screened *in vitro*, displaying IC_{50} values ranging from 35 to higher than 450 μM. It is worth noting that so far, it is the second report of fungal natural products binding to the full-length protein (1–400 amino acids). Previous reports have used a truncated model of the protein (1–300 or 1–323 amino acids), which often leads to the lack of information about the mechanism of action of the molecules. Up today, only five natural products have been reported as ligands of this macromolecule, including trodusquemine and four dimeric phenalenones from a *Talaromyces* species, the later reported by our research team, highlighting the lack of information regarding inhibitors of the full-length protein, and further supporting the medicinal chemistry performed in butyrolactone I (**1**). Furthermore, PCA of the chemical space of butyrolactone I (**1**) derivatives indicated that small differences in the structure of these ligands have a significant effect on their IC_{50} values. Molecular docking studies of butyrolactone I (**1**) and its derivatives with a homologated model of *h*PTP1B$_{1–400}$ suggested that some of these molecules may behave as allosteric modulators. Finally, after inner filter effect correction, fluorescence quenching experiments determined the binding affinity of the complex **1**-*h*PTP1B$_{1–400}$ and supported that butyrolactone I (**1**) may behave as an allosteric inhibitor of the protein. Altogether, the results from this investigation highlight the applicability of one-step semisynthetic approaches to expand the chemical space of fungal natural products and detect the important features that impact and improve their bioactivity, and the use of full-length models of PTP1B in drug discovery programs.

4. Experimental section

4.1. General experimental procedures

NMR experiments were conducted in $CDCl_3$. NMR instrumentation

was a Bruker Advance III 500 (^{1}H 500 MHZ, ^{13}C 125 MHZ) or a Bruker Ascend III 700 MHz NMR spectrometer equipped with a cryoprobe, operating at 700 MHz for ^{1}H and 175 MHz for ^{13}C. The chemical shifts are reported in ppm and are referenced to the residual solvent resonances (7.26 ppm for δ_H, and 77.16 ppm for δ_C). HR-ESI-MS data were obtained in a Thermo QExactive Plus Hybrid Quadrupole-Orbitrap mass spectrometer (ThermoFisher, San Jose, CA, USA) coupled to a Waters Acquity Ultraperformance Liquid Chromatography (UPLC) system (Waters Corp.), or a Jeol, AccuTOF JMS-T100LC mass spectrometer (HR-DART-MS). The UPLC separations were performed using an Acquity BEH C_{18} column (50 mm × 2.1 mm, internal diameter, 1.7 μm) equilibrated at 40 °C and a flow rate of 0.3 mL/min. The mobile phase consisted of a linear CH_3CN-H_2O (acidified with 0.1% formic acid) gradient starting at 15% CH_3CN to 100% CH_3CN over 8 min. The mobile phase was held for 1.5 min at 100% CH_3CN before returning to the starting conditions. HPLC separations were performed using a Waters system (2535 quaternary pump) connected to a 2707 autosampler and a 2998 PDA detector. Data acquisition and analysis were made with the Empower 3 software (Waters). Analytical and semipreparative HPLC were performed on Gemini-NX 5 μm particle size C_{18} columns (4.6 × 250 mm, and 10.0 × 250 mm for analytical and semipreparative runs, respectively; Phenomenex, Torrance, CA, USA).

4.2. Fungal strain isolation and molecular identification

IQ-046 was isolated from wetland sediment (Tamiahua-El Ídolo, Veracruz, Mexico) by Jesús Morales-Jiménez and José Rivera-Chávez. The strain was identified by Jesús Morales-Jiménez using the sequence of internal transcribed spacer (ITS) regions of the rDNA. ITS regions were amplified using the primers ITS1 (5′-GGAAGTAAAAGTCGTAACAAGG-3′) and ITS4 (5′-TCCTCCGCTTATTGATATGC-3′) by PCR.[48,49] Final concentrations for 25 μL PCR reactions were as follows: 10 ng of fungal genomic DNA, 0.8 pM of each primer, 0.2 mM dNTPs, 2.5 mM MgCl2, 1 U of Taq polymerase, and 1 × Taq polymerase buffer (Invitrogen Life Technologies, Sao Paulo, Brazil). The reaction conditions were 94 °C for 10 min; 35 cycles of 45 s at 94 °C, 45 s at 58 °C, and 60 s at 72 °C; and a final extension at 72 °C for 10 min. PCR products were purified using the QIAquick PCR purification kit (Qiagen, Valencia, CA, USA) and sequenced in an ABI PRISM 310 genetic analyzer (Applied Biosystems, Foster City, CA, USA) using the ITS1 primer.

The sequence from the ITS region of the fungal isolate IQ-046 was compared with the nonredundant GenBank library using a BLAST search.[50] A collection of taxonomically related sequences was obtained from the National Center for Biotechnology Information Taxonomy Browser. DNA sequences were aligned using CLUSTAL X,[51] edited and confirmed visually in BIOEDIT.[52] Maximum likelihood analyses were performed using PhyML.[53] The GTR + G + I model (α = 0.401 for the gamma distribution; A = 0.18, C = 0.31, G = 0.28, T = 0.23; p-inv = 0.281) was selected for the tree search. The confidence at each node was assessed by 1000 bootstrap replicates.[54] *Histoplasma capsulatum* was used as the outgroup. The sequence for the ITS region of fungal isolate IQ-046 was deposited in the GenBank database under the accession number MT254737.

4.3. Fermentation, extraction and isolation

A seed culture of the fungal strain IQ-046 was grown on potato-dextrose-agar (PDA). Then, the mycelium transferred into potato-dextrose-broth (PDB, 15 mL × 8) and incubated for seven days at rt with agitation at 100 rpm. Each seed culture was then transferred into an E-flask (250 mL) containing 10 g of autoclaved cereal (Cheerios × 8).[25] All flasks were incubated at rt for 28 days. To the large scale solid fermentation of IQ-046, 500 mL of 1:1 CH_2Cl_2-MeOH mixture was added and shaken for 24 h at 100 rpm.[55,56] Next, the solution was filtered, and 750 mL of each H_2O and CH_2Cl_2 were added to a final volume of 2 L. The mixture was stirred for 30 min and partitioned in a separatory funnel. The bottom layer was drawn off and evaporated to dryness. The solid was resuspended in 300 mL of 1:1 MeOH-CH_3CN mixture and partitioned with 300 mL of hexane in a separatory funnel. The bottom layer was evaporated to dryness.[57] The extract (2.5 g) was adsorbed onto a minimal amount of silica gel. This material was fractionated via open column chromatography, using 200 g of silica gel 230–400 mesh (Macherey-Nagel), and a gradient solvent system of hexane-EtOAc 100:0 → 0:100, to afford 28 fractions (F_1-F_{28}). Butyrolactone I (**1**) (860.2 mg) was obtained as a yellow vitreous solid from fractions F_{14}-F_{16}. Fraction F_{20} (17 mg) was subjected to semi-preparative reversed-phase chromatography on a GeminiNX C_{18} column using an isocratic system of CH_3CN-H_2O (0.1% formic acid) 45:55 for 10 min at a flow rate of 4.6 mL/min, to afford compound **2** (7.9 mg). Fraction F_{21} (~30 mg) was subjected to semipreparative HPLC using a gradient system initiated with 50:50 CH_3CN-H_2O (0.1% formic acid) to 70% CH_3CN over 30 min at a flow rate of 4.6 mL/min to generate compound **3** (8.5 mg). Fraction F_{23} (~30 mg) was resolved by semipreparative HPLC using an isocratic system of CH_3CN-H_2O (0.1% formic acid) 45:55 for 25 min at a flow rate of 4.6 mL/min, to afford compound **4** (4.6 mg). Finally, fraction F_{22} (~8 mg) was resolved by semipreparative HPLC using a gradient system initiated with 20:80 CH_3CN-H_2O (0.1% formic acid) to 80% CH_3CN over 30 min at a flow rate of 4.6 mL/min to generate compound **5** (1.3 mg).

4.3.1. Butyrolactone I (*1*)

^{1}H NMR ($CDCl_3$, 500 MHz) δ: 7.63 (2H, d, J = 8.9 Hz, H-2′, H-6′), 6.91 (2H, d, J = 8.9 Hz, H-3′, H-5′), 6.60 (1H, dd, J = 8.2, 2.2 Hz, H-6″), 6.54 (1H, d, J = 8.2 Hz, H-5″), 6.52 (1H, d, J = 2.2 Hz, H-2″), 5.99 (1H, s, OH-4′), 5.47 (1H, s, OH-4″), 5.10 (1H, dddd, J = 8.7, 5.7, 2.8 Hz, 1.4, H-8″), 3.78 (3H, s, 6-OMe), 3.56 (1H, d, J = 14.7 Hz, H-5a), 3.50 (1H, d, J = 14.7 Hz, H-5b), 3.14 (2H, d, J = 7.2 Hz, H-7″), 1.69 (3H, s, H-11″), 1.65 (3H, s, H-10″). ^{13}C NMR ($CDCl_3$, 125 MHz) δ: 169.9 (C-6), 169.5 (C-1), 156.7 (C-4′), 153.3 (C-4″), 137.4 (C-2), 134.6 (C-9″), 132.0 (C-2″), 129.7 (C-2′, C-6′), 129.4 (C-6″), 128.3 (C-3), 126.7 (C-3″), 124.8 (C-1″), 122.4 (C-1′), 121.6 (C-8″), 116.2 (C-3′, C-5′), 115.3 (C-5″), 86.3 (C-4), 53.8 (6-OMe), 38.7 (C-5), 29.3 (C-7″), 25.9 (C-11″), and 17.9 (C-10″); HR-ESI-MS, *m/z* 425.1595 $[M+H]^+$ (calcd for $C_{24}H_{25}O_7$, 425.1595).

4.3.2. Butyrolactone IV (*2*)

^{1}H NMR ($CDCl_3$, 700 MHz) δ: 7.61 (2H, d, J = 7.2 Hz, H-2′, H-6′), 6.91 (2H, d, J = 7.2 Hz, H-3′, H-5′), 6.65 (1H, brs, H-2″), 6.57 (1H, d, J = 8.2 Hz, H-6″), 6.52 (1H, d, J = 8.2 Hz, H-5″), 4.53 (dd, J = 9.4, 8.6 Hz, H-8″), 3.78 (3H, s, 6-OMe), 3.56 (1H, d, J = 14.9 Hz, H-5a), 3.49 (1H, d, J = 14.9 Hz, H-5b), 3.02 (1H, dd, J = 15.6, 8.6 Hz, H-7a''), 2.96 (1H, dd, J = 15.6, 9.4 Hz, H-7b''), 1.30 (3H, s, H-11″), 1.15 (3H, s, H-10″). ^{13}C NMR ($CDCl_3$, 175 MHz) δ: 169.8 (C-6), 169 (C-1), 159 (C-4″), 156.5 (C-4′), 137.2 (C-2), 130.2 (C-6″), 129.7 (C-2′, C-6′), 127.6 (C-3), 127.1(C-2″), 127.0 (C-3″), 124.8 (C-1″), 122.6 (C-1′), 116.2 (C-3′, C-5′), 108.6 (C-5″), 89.5 (C-8″), 86.1 (C-4), 72.1 (C-9″), 53.7 (6-OMe), 39.0 (C-5), 30.7 (C-7″), 26.3 (C-11″), and 24.0 (C-10″); HR-ESI-MS, *m/z* 458.1807 $[M+NH_4]^+$ (calcd for $C_{24}H_{28}NO_8$, 458.1809).

4.4. Semisynthesis of products *6*–*12*

4.4.1. (±)-Asperteretone B (*6*)

To a cold solution of butyrolactone I (**1**, 15 mg, 0.035 mmol) in THF (1 mL) was added 27 mL of DMC (0.32 mmol), and 1.0 mL of TBAI 78.5 mM in THF. The reaction mixture was stirred and heated at 80 °C for 6 h. The final solution was then adsorbed onto Celite and eluted with MeOH. Product **6** (3.3 mg) was purified by reverse phase (C-18) semipreparative HPLC, using an isocratic method of 50:50 CH_3CN:H_2O (0.1% formic acid) for 30 min at 4.6 mL/min, (R_t 9.5–10.5 min). The spectroscopic data were consistent with those reported in the literature. ^{1}H NMR ($CDCl_3$, 700 MHz) δ: 7.41 (2H, d, J = 8.7 Hz, H-2′, H-6′), 6.89 (2H, d, J = 8.7 Hz, H-3′, H-5′), 6.87 (1H, d, J = 7.9 Hz, H-6″), 6.86 (1H, d, brs, H-2″), 6.75 (1H, d, J = 7.9 Hz, H-5″), 5.46 (1H, s, H-4), 5.28 (1H, dddd, J = 7.2, 5.9, 2.7, 1.4 Hz, H-8″), 5.20 (1H, s, 4′-OH), 5.12 (1H, s, 4″-OH), 3.98

(1H, d, $J = 15.2$ Hz, H-5a), 3.60 (1H, d, $J = 15.2$ Hz, 5b), 3.55 (3H, s, 4-OMe), 3.32 (2H, d, $J = 7.2$ Hz, H-7″), 1.77 (3H, s, H-10″), 1.77 (3H, s, H-11″). δ: ^{13}C NMR ($CDCl_3$, 175 MHz) 171.2 (C-1), 156.5 (C-4′), 156.2 (C-3), 153.6 (C-4″), 135.3 (C-9″), 130.8 (C-2′, C-6′), 130.5 (C-2″), 129.2 (C-2), 128.3 (C-1″), 127.9 (C-6″), 127.7 (C-3″), 121.7 (C-1′), 121.6 (C-8″), 116.3 (C-5″), 115.8 (C-3′, C-5′), 102.5 (C-4), 57.3 (4-OMe), 32.0 (C-5), 29.9 (C-7″), 25.9 (C-10′), and 18.1 (C-11″); HR-DART-MS, *m/z* 381.1693 $[M+H]^+$ (calcd for $C_{23}H_{25}O_5$, 381.1697).

4.4.2. (±)-5″-Iodoasperteretone B (7)

To a cold solution of butyrolactone I (**1**, 15 mg, 0.035 mmol), in THF (1 mL) was added 27 mL of DMC (0.32 mmol), and 1.0 mL of TBAI 78.5 mM in THF. The reaction mixture was stirred and heated at 80 °C for 6 h. The final solution was then adsorbed onto Celite and eluted with MeOH. Product **7** (1.3 mg) was purified by reverse phase (C-18) semipreparative HPLC, using an isocratic method of 50:50 CH_3CN:H_2O (0.1% formic acid) for 30 min at 4.6 mL/min, (R_t 13.0–14.0 min). Compound **7** was isolated as a white solid powder. ^{1}H NMR ($CDCl_3$, 700 MHz) δ: 7.40 (2H, d, $J = 8.7$ Hz, H-2′, H-6′), 7.29 (1H, d, $J = 2.2$ Hz, H-6″), 6.91 (2H, d, $J = 8.7$ Hz, H-3′, H-5′), 6.86 (1H, d, $J = 2.2$ Hz, H-2″), 5.46 (1H, s, 4″-OH), 5.45 (1H, s, H-4), 5.25 (1H, ddq, $J = 8.8$, 5.9, 1.4 Hz, H-8″), 5.02 (1H, s, 4′-OH), 3.94 (1H, d, $J = 15.3$ Hz, H-5a), 3.57 (1H, d, $J = 15.3$ Hz, H-5b), 3.57 (3H, s, 4-OMe), 3.34 (2H, dd, $J = 5.9$ Hz, 5.8, H-7″), 1.75 (3H, d, $J = 1.3$ Hz, H-11″), 1.72 (3H, d, $J = 1.3$ Hz, H-10″). δ: ^{13}C NMR ($CDCl_3$, 175 MHz) 170.9 (C-1), 156.5 (C-4′), 155.2 (C-3), 152.2 (C-4″), 136.1 (C-6″), 134.8 (C-9″), 130.9 (C-2″), 130.8 (C-2′, C-6′), 130.1 (C-3″), 129.6 (C-2), 128.7 (C-1″), 121.6 (C-1′), 121.3 (C-8″), 115.8 (C-3′, C-5′), 102.4 (C-4), 86.4 (C-5″), 57.5 (4-OMe), 31.5 (C-5) 30.2 (C-7″), 26.0 (C-11″), 18.0 (C-10″); HR-DART-MS, *m/z* 507.0681 $[M+H]^+$ (calcd for $C_{23}H_{24}IO_5$, 507.0663).

4.4.3. (±)-Asperteretone D (8)

To a cold solution of butyrolactone I (**1**, 15 mg, 0.035 mmol), in THF (1 mL) was added 27 mL of DMC (0.32 mmol), and 1.0 mL of TBAI 78.5 mM in THF. The reaction mixture was stirred and heated at 80 °C for 6 h. The final solution was then acidified with HCl 1 M, and then adsorbed onto Celite and eluted with MeOH. Product **8** (1.3 mg) was purified by reverse phase (C-18) semipreparative HPLC, using a gradient 50:50–100:0 CH_3CN:H_2O (0.1% formic acid) over 30 min at 4.6 mL/min, (R_t 12.5–13.5 min). Compound **8** was isolated as a white powder; the spectroscopic data agreed with those previously reported in the literature. ^{1}H NMR ($CDCl_3$, 700 MHz) δ: 7.43 (2H, d, $J = 8.6$ Hz, H-2′, H-6′), 6.90 (2H, d, $J = 8.6$ Hz, H-3′, H-5′), 6.88 (1H, dd, $J = 8.4$ Hz, 2.3, H-6″), 6.81 (1H, d, $J = 2.2$ Hz, H-2″), 6.72 (1H, d, $J = 8.4$ Hz, H-5″), 5.50 (1H, s, H-4), 3.98 (1H, d, $J = 15.2$ Hz, H-5a), 3.58 (1H, d, $J = 15.2$ Hz, H-5b), 3.58 (3H, s, 4-OMe), 2.73 (2H, t, $J = 6.8$ Hz, H-7″), 1.79 (2H, t, $J = 6.8$ Hz, H-8″), 1.33 (3H, s, H-10″), 1.33 (3H, s, H-11″). δ: ^{13}C NMR ($CDCl_3$, 175 MHz) 171.1 (C-1), 156.4 (C-4′), 156.3 (C-3), 153.3 (C-4″), 130.8 (C-2′, C-6′), 129.8 (C-2″), 129.1 (C-2), 127.8 (C-6″), 127.1 (C-1″), 121.8 (C-1′), 121.6 (C-3″), 117.8 (C-5″), 115.7 (C-3′, C-5′), 102.4 (C-4), 74.5 (C-9″), 57.3 (4-OMe), 32.8 (C-8″), 31.9 (C-5), 27.0 (C-10″), 27.0 (C-11″), and 22.6 (C-7″); HR-ESI-MS, *m/z* 398.1959 $[M+NH_4]^+$ (calcd for $C_{23}H_{28}NO_5$, 398.1962).

4.4.4. Aspernolide A (9)

Compound **9** was obtained by reacting 10.1 mg of **1** (0.024 mmol) in MeOH (1 mL) with 50 μL of HCl 1 M. Aspernolide A (**9**, 4.6 mg) was purified by semipreparative reverse phase HPLC using a gradient system of 40:60–60:40 CH_3CN:H_2O (0.1% formic acid) over 30 min at a flow rate of 4.6 mL/min, (R_t 19.5–21.5 min). Compound **9** was isolated as a white powder and its spectroscopic data agreed with those reported in the literature. ^{1}H NMR ($CDCl_3$, 700 MHz) δ: 7.61 (2H, d, $J = 8.8$ Hz, H-2′, H-6′), 6.92 (2H, d, $J = 8.8$ Hz, H-3′, H-5′), 6.56 (1H, s, H-2″), 6.51 (1H, s, H-5″), 6.51 (1H, s, H-6″), 3.78 (3H, s, 6-OMe), 3.54 (1H, d, $J = 14.8$ Hz, H-5a), 3.44 (1H, d, $J = 14.8$ Hz, H-5b), 2.62 (1H, dt, $J = 16.7$, 6.8 Hz, H-7a′′), 2.59 (1H, dt, $J = 16.7$, 6.8 Hz, H-7b′′), 1.72 (1H, t, $J = 6.8$ Hz, H-8″), 1.27 (3H, s, H-10″), 1.27 (3H, s, H-11″). δ: ^{13}C NMR ($CDCl_3$, 175 MHz) 169.9 (C-6), 169.1 (C-1), 156.5 (C-4′), 153.3 (C-4″), 137.2 (C-2), 131.7 (C-2″), 129.7 (C-2′, C-6′), 129.3 (C-6″), 127.6 (C-3), 123.7 (C-1″), 122.6 (C-1′), 120.5 (C-3″), 116.8 (C-5″), 116.1 (C-3′, C-5′), 86.2 (C-4), 74.3 (C-9″), 53.7 (6-OMe), 38.8 (C-5), 32.8 (C-8″), 27.0 (C-10″), 26.9 (C-11″), and 22.4 (C-7″); HR-ESI-MS, *m/z* 442.1860 $[M+NH_4]^+$ (calcd for $C_{24}H_{28}NO_7$, 442.1860).

4.4.5. 4′,4″-Butyrolactone I dipropionate (10)

Compound **10** was obtained by reacting 10.0 mg (0.024 mmol) of **1**, with propionic anhydride (0.40 mmol) in 500 μL of pyridine. Compound **10** (4.5 mg) was purified by reverse phase semipreparative HPLC using a gradient system of 40:60–60:40 CH_3CN:H_2O (0.1% formic acid) over 30 min at a flow rate of 4.6 mL/min, (R_t 10.5–12.0 min). ^{1}H NMR ($CDCl_3$, 700 MHz) δ: 7.72 (2H, d, $J = 8.8$ Hz, H-2′, H-6′), 7.20 (2H, d, $J = 8.8$ Hz, H-3′, H-5′), 6.78 (1H, d, $J = 8.2$ Hz, H-5″), 6.71 (1H, dd, $J =$, 8.2, 2.2 Hz, H-6″), 6.66 (1H, d, $J = 2.2$ Hz, H-2″), 5.00 (1H, tt, $J = 7.2$, 1.5 Hz, H-8″), 3.79 (3H, s, 6-OMe), 3.63 (1H, d, $J = 14.7$ Hz, H-5a), 3.54 (1H, d, $J = 14.7$ Hz, H-5a), 3.04 (2H, d, $J = 7.2$ Hz, H-7″), 1.67 (3H, d, $J = 1.3$ Hz, H-11″), 1.58 (3H, d, $J = 1.3$ Hz, H-10″), 2.65 (2H, q, $J = 7.6$ Hz, —COOC$\underline{H}_2$CH$_3$), 1.29 (2H, t, $J = 7.6$ Hz, —COOCH$_2$C$\underline{H}_3$), 2.57 (2H, q, $J = 7.6$ Hz, —COOC$\underline{H}_2$CH$_3$), 1.24 (2H, t, $J = 7.6$ Hz, —COOCH$_2$C$\underline{H}_3$). δ: ^{13}C NMR ($CDCl_3$, 175 MHz) 169.6 (C-6), 168.6 (C-1), 151.3 (C-4′), 148.3 (C-4″), 138.9 (C-2), 133.4 (C-3″), 133.3 (C-9″), 132.1 (C-2″), 130.5 (C-1″), 129.1 (C-6″), 129.0 (C-2′, C-6′), 127.2 (C-1′), 126.5 (C-3), 122.4 (C-3′, C-5′), 121.9 (C-5″), 121.4 (C-8″), 85.8 (C-4), 53.8 (6-OMe), 38.9 (C-5), 28.5 (C-7″), 25.8 (C-11″), 17.9 (C-10″), 173.0 (—$\underline{C}$OOCH$_2$CH$_3$), 27.7 (—COO$\underline{C}$H$_2$CH$_3$), 9.3 (—COOCH$_2$$\underline{C}H_3$), 172.7 (—$\underline{C}$OOCH$_2CH_3$), 27.9 (—COO$\underline{C}H_2CH_3$), and 9.2 (—COOCH$_2$$\underline{C}H_3$); HR-ESI-MS, *m/z* 554.2383 $[M+NH_4]^+$ (calcd for $C_{30}H_{36}NO_9$, 554.2384).

4.4.6. $\Delta^{7'',8''}$-9″-hydroxy-4′,4′-butyrolactone I dipropionate (11)

Compound **11** was obtained by reacting 10.0 mg (0.024 mmol) of **1**, with propionic anhydride (0.40 mmol) in 500 μL of pyridine. Compound **11** (1.5 mg) was purified by reverse phase semipreparative HPLC using a gradient system of 40:60–60:40 CH_3CN:H_2O (0.1% formic acid) over 30 min at a flow rate of 4.6 mL/min, (R_t 8.5–9.5 min). ^{1}H NMR ($CDCl_3$, 700 MHz) δ: 7.72 (2H, d, $J = 8.8$ Hz, H-2′, H-6′), 7.21 (2H, d, $J = 8.8$ Hz, H-3′, H-5′), 6.87 (1H, s, H-2″), 6.84 (1H, d, $J = 1.3$ Hz, H-5″), 6.84 (1H, d, $J = 1.3$ Hz, H-6″), 6.41 (2H, d, $J = 16.4$ Hz, H-7″), 5.90 (1H, d, $J = 16.4$ Hz, H-8″), 3.82 (3H, s, 6-OMe), 3.64 (1H, d, $J = 14.8$ Hz, H-5a), 3.59 (1H, d, $J = 14.8$ Hz, H-5b), 1.36 (3H, s, H-10″), 1.36 (3H, s, H-11″), 2.63 (2H, q, $J = 7.6$ Hz, —COOC$\underline{H}_2$CH$_3$), 1.29 (2H, t, $J = 7.6$ Hz, —COOCH$_2$C$\underline{H}_3$), 2.58 (2H, q, $J = 7.6$ Hz, —COOC$\underline{H}_2$CH$_3$), 1.26 (2H, t, $J = 7.6$ Hz, —COOCH$_2$C$\underline{H}_3$). δ: ^{13}C NMR ($CDCl_3$, 175 MHz) 169.5 (C-6), 168.6 (C-1), 151.3 (C-4′), 147.5 (C-4″), 138.9 (C-2), 136.2 (C-8″), 130.7 (C-1″), 130.6 (C-6″), 129.0 (C-2′, C-6′), 128.6 (C-3), 128.6 (C-3″), 127.3 (C-1′), 123.4 (C-7″), 122.6 (C- 3′, C-5′), 122.4 (C-2″), 122.4 (C-5″), 85.8 (C-4), 82.3 (C-9″), 53.9 (6-OMe), 38.7 (C-5), 24.5 (C-11″), 24.4 (C-10″), 173.1 (—$\underline{C}$OOCH$_2$CH$_3$), 27.8 (—COO$\underline{C}$H$_2$CH$_3$), 9.4 (—COOCH$_2$$\underline{C}H_3$), 172.9 (—$\underline{C}$OOCH$_2CH_3$), 27.9 (—COO$\underline{C}H_2CH_3$), and 9.1 (—COOCH$_2$$\underline{C}H_3$); HR-ESI-MS, *m/z* 570.2332 $[M+NH_4]^+$ (calcd for $C_{30}H_{36}NO_{10}$, 570.2333).

4.4.7. 3′,5′,5″,8″-Tetrabromoaspernolide A (12)

To a solution of butyrolactone I (**1**, 10 mg, 0.024 mmol) in CH_2Cl_2-MeOH, 1:1, was added Br_2 in excess (50 μL, 2.7 mmol in 500 μL of CH_2Cl_2), and stirred for 3 h at rt. 3′,5′,5″,8″-tetrabromoaspernolide A (**12**, 1.8 mg) was purified by semipreparative reverse phase HPLC, using an isocratic method of 40:30:30 CH_3CN-MeOH-H_2O (0.1% formic acid) at a flow rate of 4.6 mL/min. ^{1}H NMR ($CDCl_3$, 700 MHz) δ: 7.79 (2H, s, H-2′, H-6′), 6.83 (1H, d, $J = 2.1$ Hz, H-6″), 6.55 (1H, d, $J = 2.1$ Hz, H-2″), 4.18 (1H, dd, $J = 9.2$, 5.6 Hz, H-8″), 3.83 (3H, s, 6-OMe), 3.51 (1H, d, $J = 15.0$ Hz, H-5a), 3.34 (1H, d, $J = 15.0$ Hz, H-5b), 3.26 (1H, dd, $J = 17.0$, 6.0 Hz, H-7a′′), 3.10 (1H, dd, $J = 17.0$, 9.2 Hz, H-7b′′), 1.55 (3H, s, H-11″), 1.40, (3H, s, H-10″). δ: ^{13}C NMR ($CDCl_3$, 175 MHz) 169.1 (C-6), 168.0 (C-1), 150.3 (C-4′), 149.1 (C-4″), 138.9 (C-2), 133.4 (C-6″), 131.4

(C-2′, C-6′), 130.2 (C-2″), 125.6 (C-3), 124.5 (C-1′), 124.5 (C-1″), 121.1 (C-3″), 111.1 (C-5″), 110.7 (C-3′, C-5′), 85.7 (C-4), 78.5 (C-9″), 54.0 (6-OMe), 51.7 (C-8″), 38.5 (C-5), 34.3 (C-7″), 27.1 (C-11″), and 21.9 (C-10″); HR-ESI-MS, *m/z* 734.7877 $[M - H]^-$ (calcd for $C_{24}H_{19}O_7Br_4$, 734.7870).

4.5. *h*PTP1B$_{1–400}$, expression and purification

Human wild-type PTP1B (*h*PTP1B$_{1–400}$, residues 1–400) containing an *N*-terminal 6 × His tag was cloned into a pET28 vector. The plasmid was transformed into an *E. coli* Rosetta (DE3) pLysS strain and grown using LB media. Protein expression was induced using 1 mM IPTG at 20 °C for 16 h. Purification of *h*PTP1B$_{1–400}$ was carried out following the procedure previously described by Jiménez-Arreola, et al. 2020.[7] Briefly, cells were resuspended in lysis buffer (50 mM HEPES pH 7.2, 150 mM NaCl, 10 mM imidazole, 2 mM TCEP) and sonicated in an ice bath (4 °C). Lysates were then centrifuged and purified using affinity chromatography, by 50 mM HEPES pH 7.4, 100 mM NaCl, 300 mM imidazole, and 1.5 mM DTT, with subsequent buffer exchange using 50 mM HEPES pH 7.4, 100 mM NaCl, and 1.5 mM DTT. The protein was used immediately or stored at − 20 °C in 50 mM HEPES pH 7.4, 100 mM NaCl, 2 mM DTT, and 4% glycerol.[34,58]

4.6. *h*PTP1B$_{1–400}$ inhibition assay

Pure compounds and ursolic acid (positive control) were dissolved in DMSO. Aliquots of 0–10 μL of testing materials (in triplicate) were incubated for 10 min with 5 μL of enzyme stock solution (3 μM) in 50 mM HEPES pH 6.8, 100 mM NaCl, 1.5 mM DTT. After incubation, 10 μL of the substrate (*p*-NPP 30 mM, Sigma-Aldrich) was added and incubated for 20 min at 37 °C, and the absorbance at 405 nm was determined. All assays were performed in a final volume of 100 μL. The IC_{50} values were calculated by regression analysis using Eq. (1), with GraphPad Prism.

$$\%Inh = \frac{A_{100}}{1 + \left(\frac{I}{IC_{50}}\right)^S} \quad (1)$$

4.7. Computational details

4.7.1. Proteins and ligands

Polar hydrogens and charges (Kollman) were allocated to the homologated model for *h*PTP1B$_{1-400}$ using AutoDockTools (ADT) 1.5.6, and the files saved in .pdbqt format for their use in AutoGrid 4.0 and AutoDock 4.0 interfaces. All docked compounds were built and energy-optimized using Spartan 10 using a semi-empiric method (PM3). The ligands were prepared in ADT 1.5.6 by adding the Gasteiger-Marsili charges.

4.7.2. Molecular docking

Simulations were performed using AutoDock 4.0. Previously, the docking protocols were validated to ensure the integrity of the data. In this regard, trodusquemine was used as a probe to validate the simulations generated for *h*PTP1B$_{1-400}$.[7] After validation, a blind docking was performed for each ligand at the interface as the first ligand binding position in a grid box with dimensions of 126 × 126 × 126 Å. Docking simulations were performed with Lamarckian Genetic Algorithm calculations of 100 runs. The obtained poses were analyzed with ADT 1.5.6 using cluster analysis, and visualized with PyMOL.

4.8. Steady-state fluorescence quenching experiments

All measurements were carried out in an Agilent Cary Eclipse spectrometer with continuous stirring at 20 °C. The *h*PTP1B$_{1-400}$ (0.5 μM) was incubated in buffer (50 mM HEPES pH 6.8, 100 mM NaCl, 1.5 mM DTT). The excitation wavelength was 280 nm, and the emission wavelengths from 300 to 500 nm were recorded. The inner filter effect due to the absorption of butyrolactone I (**1**) at the excitation and emission wavelengths was corrected by treating the fluorescence data with Eq. (2), "where F_{cor} and F_{obs} are the corrected and measured fluorescence intensities, respectively, and A_{ex} and A_{em} are the differences in the absorbance values of the sample upon the addition of the ligand at the excitation (280 nm) and emission (300–400 nm) wavelengths, respectively."[45]

$$F_{cor} = F_{obs} 10^{\frac{(A_{ex}+A_{em})}{2}} \quad (2)$$

The saturation degree of *h*PTP1B$_{1-400}$ with butyrolactone I (**1**), and the k_a for the **1**-*h*PTP1B$_{1-400}$ complex was calculated by non-linear regression utilizing Eq. (3), where *F* is the measured fluorescence, and F_0 and F_c are the fluorescence in the absence of the ligand and the fully saturated protein, respectively, $[P]_t$ and $[L]_t$ are the total protein and total ligand concentration, and $k_d = (1/k_a)$ is the dissociation constant.[45]

$$\frac{F_0 - F}{F_0 - F_c} = \frac{[P]_t + [L]_t + k_d - \sqrt{\left([P]_t + [L]_t + k_d\right)^2 - 4[P]_t[L]_t}}{2[P]_t} \quad (3)$$

Declaration of Competing Interest

The authors declare that they have no known competing financial interests or personal relationships that could have appeared to influence the work reported in this paper.

Acknowledgments

This work was supported by a grant from DGAPA, PAPIIT, UNAM (IA200818/IA203220). This research received partial financial support from CONACyT, through infrastructure project no. 295057. The authors would like to thank Dr. Beatriz Quiroz-García, Dra. María del Carmen García-González, and Dr. Celia Bustos-Brito (Instituto de Química, UNAM) for the collection of spectroscopic and spectrometric data, and technical assistance. This study made use of UNAMs NMR Laboratory: LURMN at IQ-UNAM, which is funded by CONACyT-Mexico (Project: 0224747) and UNAM, as well as the instrumentation acquired through the BGSI-IQ node. J. R-C. would like to thank MSc. Tyler N. Graff and Jacklyn M. Gallagher, and Dr. Huzefa Raja for their assistance in the revision of the manuscript.

Appendix A. Supplementary material

1D NMR (^{1}H and ^{13}C), 2D NMR (COSY, HSQC, and HMBC), and HRMS data for compounds **1**-**12**. Summarized 1D NMR data for compounds **1**, **2**, and **6**-**12**. Molecular docking for compounds **1**, **2**, and **6**-**12**. Supplementary data to this article can be found online at https://doi.org/10.1016/j.bmc.2020.115817.

References

1 Tamrakar AK, Maurya CK, Rai AK. PTP1B inhibitors for type 2 diabetes treatment: a patent review (2011–2014). *Expert Opin Ther Pat*. 2014;24:1101–1115.
2 Lessard L, Stuible M, Tremblay ML. The two faces of PTP1B in cancer. *BBA*. 2010; 1804:613–619.
3 Bollu LR, Mazumdar A, Savage MI, Brown PH. Molecular pathways: Targeting protein tyrosine phosphatases in cancer. *Clin Cancer Res*. 2017;23:2136–2142.
4 Zhang S, Zhang ZY. PTP1B as a drug target: recent developments in PTP1B inhibitor discovery. *Drug Discovery Today*. 2007;12:373–381.
5 Verma M, Gupta SJ, Chaudhary A, Garg VK. Protein tyrosine phosphatase 1B inhibitors as antidiabetic agents – a brief review. *Bioorg Chem*. 2017;70:267–283.
6 Jin J, Ye X, Boateng D, et al. Identification and characterization of potent and selective inhibitors targeting protein tyrosine phosphatase 1B (PTP1B). *Bioorg Med Chem Lett*. 2019;29:2358–2363.
7 Jiménez-Arreola BS, Aguilar-Ramírez E, Cano-Sánchez P, et al. Dimeric phenalenones from *Talaromyces* sp. (IQ-313) inhibit hPTP1B1-400: insights into mechanistic kinetics from *in vitro* and *in silico* studies. *Bioorg Chem*. 2020;101: 103893.

8 Zargari F, Lotfi M, Shahraki O, Nikfarjam Z, Shahraki J. Flavonoids as potent allosteric inhibitors of protein tyrosine phosphatase 1B: molecular dynamics simulation and free energy calculation. *J Biomol Struct Dyn*. 2018;36:4126–4142.
9 Wiesmann C, Barr KJ, Kung J, et al. Allosteric inhibition of protein tyrosine phosphatase 1B. *Nat Struct Mol*. 2004;11:730–737.
10 Zhang ZY, Lee SY. PTP1B inhibitors as potential therapeutics in the treatment of type 2 diabetes and obesity. *Expert Opin Invest Drugs*. 2003;12:223–233.
11 Kiriyama N, Nitta K, Sakaguchi Y, Taguchi Y, Yamamoto Y. Studies on the metabolic products of *Aspergillus terreus*. III. Metabolites of the dtrain IFO 8835. (1). *Chem Pharm Bull*. 1977;25:2593–2601.
12 Rao KV, Sadhukhan AK, Veerender M, et al. Butyrolactones from *Aspergillus terreus*. *Chem Pharm Bull*. 2000;48:559–562.
13 Alberts AW, Chen J, Kuron G, et al. Mevinolin: a highly potent competitive inhibitor of hydroxymethylglutaryl-coenzyme A reductase and a cholesterol-lowering agent. *PNAS*. 1980;77:3957.
14 Wang Y, Zheng J, Liu P, Wang W, Zhu W. Three new compounds from *Aspergillus terreus* PT06-2 grown in a high salt medium. *Mar Drugs*. 2011;9:1368–1378.
15 Chen J, Li J, Zhu L, et al. Total synthesis and structure revision of chrysamide B. *Org Chem Front*. 2018;5:3402–3405.
16 Chen S, Wang J, Lin X, et al. three dimeric nitrophenyl trans-epoxyamides produced by the deep-sea-derived fungus *Penicillium chrysogenum* SCSIO41001. *Org Lett*. 2016;18:3650–3653.
17 Ouk S, Thiébaud S, Borredon E, Le Gars P. High performance method for O-methylation of phenol with dimethyl carbonate. *Appl Catal A-Gen*. 2003;241:227–233.
18 Liu M, Qi C, Sun W, et al. α-Glucosidase inhibitors from the coral-associated fungus *Aspergillus terreus*. *Front Chem*. 2018;6:422.
19 Tundo P, Musolino M, Aricò F. The reactions of dimethyl carbonate and its derivatives. *Green Chem*. 2018;20:28–85.
20 Krapcho AP, Glynn GA, Grenon BJ. The decarbethoxylation of geminal dicarbethoxy compounds. *TetrahedronLett*. 1967;3:215–217.
21 Sun K, Zhu G, Hao J, Wang Y, Zhu W. Chemical-epigenetic method to enhance the chemodiversity of the marine algicolous fungus, *Aspergillus terreus* OUCMDZ-2739. *Tetrahedron*. 2018;74:83–87.
22 Parvatkar RR, D'Souza C, Tripathi A, Naik CG. Aspernolides A and B, butenolides from a marine-derived fungus *Aspergillus terreus*. *Phytochemistry*. 2009;70:128–132.
23 Dewi RT, Tachibana S, Darmawan A. Effect on α-glucosidase inhibition and antioxidant activities of butyrolactone derivatives from *Aspergillus terreus* MC751. *Med Chem Res*. 2014;23:454–460.
24 Chung W-j, Vanderwal CD. Stereoselective halogenation in natural product synthesis. *Angew Chem Int Ed*. 2016;55:4396–4434.
25 Rivera-Chávez J, Raja HA, Graf TN, Burdette JE, Pearce CJ, Oberlies NH. Biosynthesis of fluorinated peptaibols using a site-directed building block Incorporation approach. *J Nat Prod*. 2017;80:1883–1892.
26 Gribble GW. Biological activity of recently discovered halogenated marine natural products. *Mar Drugs*. 2015;13:4044–4136.
27 Neumann CS, Fujimori DG, Walsh CT. Halogenation strategies in natural product biosynthesis. *Chem Biol*. 2008;15:99–109.
28 Cavallo G, Metrangolo P, Milani R, et al. The halogen bond. *Chem Rev*. 2016;116:2478–2601.
29 Wilcken R, Zimmermann MO, Lange A, Joerger AC, Boeckler FM. Principles and applications of halogen bonding in medicinal chemistry and chemical biology. *J Med Chem*. 2013;56:1363–1388.
30 Jiang S, Zhang L, Cui D, et al. The Important role of halogen bond in substrate selectivity of enzymatic catalysis. *Sci Rep*. 2016;6:34750.
31 Marcelo Zaldini H, Suellen Melo TC, Diogo Rodrigo MM, Walter Filgueira de Azevedo J, Ana Cristina Lima L. Halogen atoms in the modern medicinal chemistry: hints for the drug design. *Curr Drug Targets*. 2010;11:303–314.
32 Jollow DJ, Mitchell JR, Zampaglione N, Gillette JR. Bromobenzene-induced liver necrosis. Protective role of glutathione and evidence for 3,4-bromobenzene oxide as the hepatotoxic metabolite. *Pharmacology*. 1974;11:151–169.
33 Dewachter P, Mouton-Faivre C. Allergie aux médicaments et aliments iodés : la séquence allergénique n'est pas l'iode. *La Presse Médicale*. 2015;44:1136–1145.
34 Krishnan N, Koveal D, Miller DH, et al. Targeting the disordered C terminus of PTP1B with an allosteric inhibitor. *Nat Chem Biol*. 2014;10:558–566.
35 Cerón-Romero L, Paoli P, Camici G, et al. In vitro and in silico PTP-1B inhibition and in vivo antidiabetic activity of semisynthetic moronic acid derivatives. *Bioorg Med Chem*. 2016;26:2018–2022.
36 Guzmán-Ávila R, Flores-Morales V, Paoli P, et al. Ursolic acid derivatives as potential antidiabetic agents: *In vitro*, *in vivo*, and *in silico* studies. *Drug Dev Res*. 2018;79:70–80.
37 Ramírez-Espinosa JJ, Rios MY, Paoli P, et al. Synthesis of oleanolic acid derivatives: in vitro, in vivo and in silico studies for PTP-1B inhibition. *Eur J Med Chem*. 2014;87:316–327.
38 Han W, Cai J, Zhong W, et al. Protein tyrosine phosphatase 1B (PTP1B) inhibitorsfrom the deep-sea fungus *Penicillium chrysogenum* SCSIO 07007. *Bioorg Chem*. 2020;96:103646.
39 Huo C, Lu X, Zheng Z, et al. Azaphilones with protein tyrosine phosphatase inhibitory activity isolated from the fungus *Aspergillus deflectus*. *Phytochemistry*. 2020;170:112224.
40 Kim D-C, Minh Ha T, Sohn JH, Yim JH, Oh H. Protein tyrosine phosphatase 1B inhibitors from a marine-derived fungal strain *Aspergillus* sp. SF-5929. *Nat Prod Res*. 2020;34:675–682.
41 Wen C-N, Chen H-P, Zhao Z-Z, et al. Two new γ-lactones from the cultures of basidiomycete *Lenzites betulinus*. *Phytochem Lett*. 2017;20:9–12.
42 Gubiani JR, Wijeratne EMK, Shi T, et al. An epigenetic modifier induces production of (10′S)-verruculide B, an inhibitor of protein tyrosine phosphatases by *Phoma* sp. nov. LG0217, a fungal endophyte of *Parkinsonia microphylla*. *Bioorg Med Chem*. 2017;25:1860–1866.
43 Lakowicz JR. *Principles of fluorescence spectroscopy*. 3rd ed. Springer Science & Business Media; 2013.
44 Akbar SM, Sreeramulu K, Sharma HC. Tryptophan fluorescence quenching as a binding assay to monitor protein conformation changes in the membrane of intact mitochondria. *J Bioenerg Biomembr*. 2016;48:241–247.
45 Bakar KA, Feroz SR. A critical view on the analysis of fluorescence quenching data for determining ligand–protein binding affinity. *Sprectrochim Acta A*. 2019;223:117337.
46 Fonin AV, Sulatskaya AI, Kuznetsova IM, Turoverov KK. Fluorescence of dyes in solutions with high absorbance. Inner filter effect correction. *PLos One*. 2014;9:e103878.
47 Rivera-Chávez J, Bustos-Brito C, Aguilar-Ramírez E, et al. Hydroxy-neo-clerodanes and 5,10-seco-neo-clerodanes from *Salvia decora*. *J Nat Prod*. 2020;83:2212–2220.
48 Gardes M, Bruns TD. ITS primers with enhanced specificity for basidiomycetes-application to the identification of mycorrhizae and rusts. *Mol Ecol*. 1993;2:113–118.
49 Innis MA, Gelfand DH, Sninsky JJ, White TJ. *PCR protocols: a guide to methods and applications*. 3rd ed. Academic Press; 1990.
50 Altschul SF, Madden TL, Schäffer AA, et al. Gapped BLAST and PSI-BLAST: a new generation of protein database search programs. *Nucleic Acids Res*. 1997;25:3389–3402.
51 Thompson JD, Gibson TJ, Plewniak F, Jeanmougin F, Higgins DG. The CLUSTAL_X windows interface: flexible strategies for multiple sequence alignment aided by quality analysis tools. *Nucleic Acids Res*. 1997;25:4876–4882.
52 Hall TA. *Nucleic acids symposium series*. 1999;vol. 41:95–98.
53 Guindon S, Dufayard J-F, Lefort V, Anisimova M, Hordijk W, Gascuel O. New algorithms and methods to estimate maximum-likelihood phylogenies: assessing the performance of PhyML 3.0. *Syst Biol*. 2010;59:307–321.
54 Hillis DM, Bull JJ. An empirical test of bootstrapping as a method for assessing confidence in phylogenetic analysis. *Syst Biol*. 1993;42:182–192.
55 Ayers S, Graf TN, Adcock AF, et al. Resorcylic acid lactones with cytotoxic and NF-kappaB inhibitory activities and their structure-activity relationships. *J Nat Prod*. 2011;74:1126–1131.
56 Paguigan ND, Raja HA, Day CS, Oberlies NH. Acetophenone derivatives from a freshwater fungal isolate of recently described *Lindgomyces madisonensis* (G416). *Phytochemistry*. 2016;126:59–65.
57 El-Elimat T, Figueroa M, Raja HA, et al. Biosynthetically distinct cytotoxic polyketides from *Setophoma terrestris*. *Eur J Org Chem*. 2015;2015:109–121.
58 Krishnan N, Bonham CA, Rus IA, et al. Harnessing insulin- and leptin-induced oxidation of PTP1B for therapeutic development. *Nat Commun*. 2018;9:283.